NANO LETTERS

Letter

pubs.acs.org/NanoLett

Kinetics of Initial Lithiation of Crystalline Silicon Electrodes of Lithium-Ion Batteries

Matt Pharr,[†] Kejie Zhao,[†] Xinwei Wang,[‡] Zhigang Suo,[†] and Joost J. Vlassak*,[†]

[†]School of Engineering and Applied Sciences and [‡]Department of Chemistry and Chemical Biology, Harvard University, Cambridge, Massachusetts 02138, United States

Supporting Information

ABSTRACT: Electrochemical experiments were conducted on {100}, {110}, and {111} silicon wafers to characterize the kinetics of the initial lithiation of crystalline Si electrodes. Under constant current conditions, we observed constant cell potentials for all orientations, indicating the existence of a phase boundary that separates crystalline silicon from the amorphous lithiated phase. For a given potential, the velocity of this boundary was found to be faster for {110} silicon than for the other two orientations. We show that our measurements of varying phase boundary velocities can accurately account for anisotropic morphologies and fracture developed in crystalline silicon nanopillars. We also present a kinetic model by considering the redox reaction at the electrolyte/lithiated silicon interface, diffusion of lithium through the lithiated phase, and the chemical reaction at the lithiated silicon/crystalline silicon interface. From this model, we quantify the rates of the reactions at the interfaces and estimate a lower bound on the diffusivity through the lithiated silicon phase.

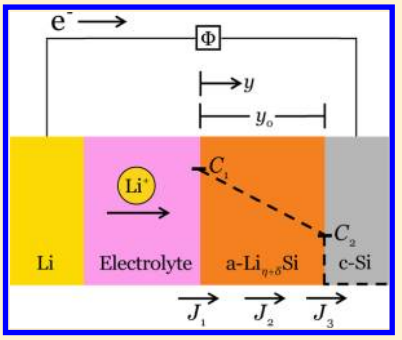

KEYWORDS: *Lithium-ion batteries, silicon, kinetics, plasticity*

Lithium-ion batteries already dominate the market as the power source for portable electronics and are beginning to find applications in electric vehicles.[1,2] Ongoing research involves the development of systems with high energy density, long cycle life, low cost, and safe operation.[3,4] Of the potential materials for anodes, silicon can host an extremely large amount of lithium, making it one of the most promising candidates.[5] However, associated with its large capacity, insertion of lithium into silicon causes large volumetric expansion of approximately 300%.[6] Under constraint, this enormous expansion can result in large mechanical stress and fracture, leading to loss of active material and degradation of the capacity of the electrode.[6] Fortunately, this mechanical damage can be mitigated through nanostructuring of the silicon anodes. Successful examples include nanowires,[7,8] thin films,[9−13] nanoporous structures,[14] and hollow nanoparticles.[15,16] Specifically, recent experiments and theories indicate that one can prevent fracture by taking advantage of lithiation-induced plasticity.[12,17−22] To develop such nanostructured anodes, it is imperative to understand the interplay among the electrochemical driving forces and the resulting mechanisms of lithiation-induced deformation, stress, and fracture.

Numerous nanostructured electrodes have been fabricated from crystalline silicon. During the initial lithiation process, crystalline silicon and lithium react at room temperature, forming an amorphous phase of lithiated silicon.[7,23−32] First-principles calculations have revealed many atomic details of this phase transformation.[23,24] Likewise, various experimental techniques have provided insight into this amorphization process.[25−28] For example, Chon et al. have demonstrated that the phase boundary between {100} crystalline silicon and amorphous lithiated silicon is atomically sharp.[29] Additionally, Liu et al. have observed that under a constant potential the motion of the phase boundary between crystalline silicon and amorphous lithiated silicon is linear in time along the [112] direction.[30] This latter experiment indicates that the rate of lithiation is not limited by diffusion through the lithiated phase but instead by short-range atomic processes at the phase boundary. These processes include breaking Si−Si bonds and forming Li−Si bonds. Further evidence of this phenomenon was provided by the observation of lithiated silicon of anisotropic morphologies, which suggest that the reaction at the phase boundary is fastest in the ⟨110⟩ direction of crystalline silicon.[30−32] In a previous theoretical study, we proposed that the observed anisotropic morphologies are due to the variation in the short-range atomic processes at the reaction fronts in different crystallographic orientations.[33] A similar theoretical analysis was proposed by Yang et al.[34] In general, any of a number of kinetic processes may be rate-limiting or multiple kinetic processes can significantly contribute to the overall kinetics of lithiation. Moreover, experimental measurements of varying phase boundary velocities for different crystallographic orientations are lacking.

To provide insight into the pertinent kinetic processes, we present an experimental study quantifying the kinetics of the initial lithiation of crystalline silicon. Crystalline silicon wafers of {100}, {110}, and {111} orientations were lithiated at

Received: July 31, 2012
Published: August 13, 2012

dx.doi.org/10.1021/nl302841y | *Nano Lett.* 2012, 12, 5039−5047

various currents, and the response of the potential was measured. To interpret these data, we have constructed a kinetic model that considers three kinetic processes in series: the redox reaction at the electrolyte/lithiated silicon interface, the diffusion of lithium through the lithiated phase, and the chemical reaction at the lithiated silicon/crystalline silicon interface. Using this model and experimental data, we can determine which kinetic processes are the most important. In particular, from our experiments we can quantify the rates of reactions at the interfaces as a function of crystal orientation. Additionally, we can provide a lower bound on the diffusivity of lithium through the lithiated silicon phase. Using the measured reaction rates, we have implemented a model of concurrent reaction and plasticity into the finite element software ABAQUS. This simulation accurately predicts anisotropic morphological evolution and anisotropic fracture during initial lithiation of crystalline silicon nanopillars of various axial orientations.

Figure 1 shows a typical response of the potential to a series of applied currents for a {110} Si wafer. When a certain

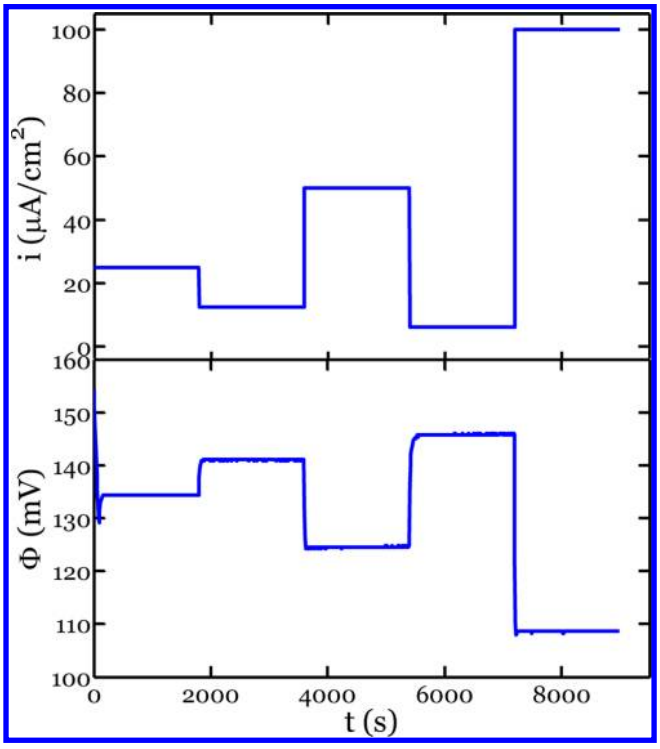

Figure 1. Typical sequence of applied current density, *i*, and measured response of the potential versus Li/Li$^+$, Φ, for a {110} Si wafer.

constant level of current density is applied for some duration of time, the measured potential of Si vs Li/Li$^+$ reaches a particular value very quickly and remains at this value for the remainder of the time. The measured potential provides information about the concentration of lithium in the electrode at the interface with the electrolyte. For two-phase coexistence, lithium insertion is accommodated by the growth of the lithium-rich phase at the expense of the lithium-poor phase. As a result, the concentration in the electrode at the interface with the electrolyte is fixed, rendering the potential constant in time for a constant current density. These two-phase plateaus are evident for all three tested orientations (Figure 1, Supporting Information Figures S1, S2), suggesting the coexistence of crystalline silicon (c-Si) and amorphous lithiated silicon(a-Li$_\eta$Si) for all three orientations. This result agrees in part with a previous work in which the boundary separating these two phases has been found to be atomically sharp for a {100} wafer.[29]

Figure 2 shows the measured plateau potentials as a function of the applied current density for all of the samples. The solid

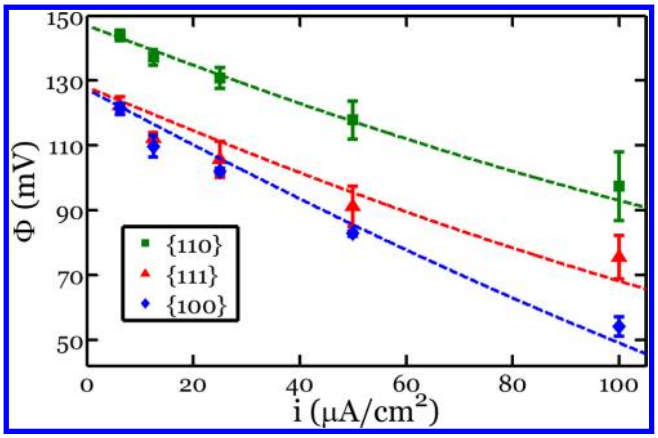

Figure 2. Measured potential versus Li/Li$^+$, Φ, as a function of applied current density, *i*, for all three orientations. The solid symbols represent the mean of the tested samples, and the error bars represent ±1 standard deviation from the mean. The dashed lines represent fits from the kinetic model.

symbols represent the mean of three samples for the given crystallographic orientation, and the error bars represent ±1 standard deviation from the mean. The variation from sample to sample is quite small, demonstrating the reproducibility of the experiment.

Although Si transforms to numerous Li−Si crystalline phases at elevated temperatures,[35] it has been shown that electrochemical lithiation of Si at room temperature results in a metastable amorphous Li$_\eta$Si phase, where $\eta \approx 3.5$.[36] It is likely that this phase exists over a finite range of lithium concentrations depending on the applied potential. However, assuming a composition of Li$_{3.5}$Si and accounting for the corresponding volume expansion $\beta = \Omega_{Li3.5Si}/\Omega_{Si} = 3.21$,[37] we have calculated the expected thickness for the current history corresponding to these experiments. These predicted thicknesses were then compared to the measured thicknesses using the SEM, and the values were in good agreement. Evidently, the velocity of the phase boundary is directly correlated with the applied current density. Hence, in our experiments one can think of the current density, for example, the horizontal axis in Figure 2, as the velocity of the moving phase boundary. Thus, Figure 2 shows that the {110} Si wafers are the "fastest" for a given potential. For instance, at 120 mV vs Li/Li$^+$ the interpolated average current densities for the {110}, {100}, and {111} Si wafers are 47.1, 7.4, and 7.7 μA/cm^2, respectively. Such discrepancy in the velocities has important ramifications for lithiation of crystalline silicon structures with various crystal facets exposed. For instance, these measurements of varying phase boundary velocities can accurately account for anisotropic morphologies and fracture patterns developed in crystalline silicon nanopillars of various axial orientations, as will be discussed later.

dx.doi.org/10.1021/nl302841y | *Nano Lett.* 2012, 12, 5039−5047

Figure 3 illustrates an electrochemical cell in which crystalline silicon and metallic lithium react and form an amorphous phase of lithiated silicon

$$(\eta + \delta)\mathrm{Li} + \mathrm{Si} = \mathrm{Li}_{\eta+\delta}\mathrm{Si} \quad (1)$$

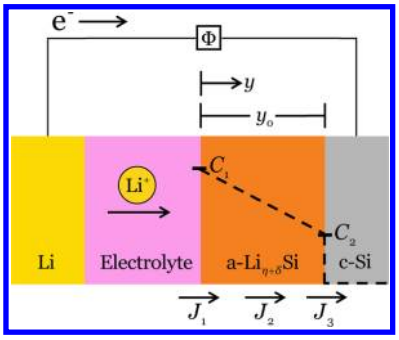

Figure 3. In an electrochemical cell, crystalline silicon and lithium react at room temperature, forming an amorphous phase of lithiated silicon. The concentrations C_1 and C_2 represent the concentration of lithium in the lithiated silicon phase at the given interfaces. The dashed line represents the variation of the concentration of lithium as a function of position in the Si electrode. The position in the a-$Li_{\eta+\delta}Si$ is denoted by y and the total thickness of the layer by y_0. The J_i denote the fluxes of lithium at various positions: J_1 at the interface between the electrolyte and the lithiated silicon phase, J_2 in the lithiated silicon phase, J_3 at the phase boundary between lithiated silicon and crystalline silicon.

The two electrodes are connected through a conducting wire and an electrolyte. The conducting wire may be connected to an external voltage source. At the interface between the metallic lithium electrode and the electrolyte, lithium atoms dissociate into lithium ions and electrons. Lithium ions pass through the electrolyte while electrons pass through the conducting wire. Upon reaching the silicon electrode, lithium ions and electrons recombine into lithium atoms. We expect that this latter process occurs at the interface between the electrolyte and the a-$Li_\eta Si$, as the silicon samples have fairly large electric conductivity (see the Experimental Methods) and lithiated silicon has even larger conductivity because of its metallic-like properties.[23,37] Lithium atoms then diffuse through the lithiated silicon and react with the crystalline silicon (at the reaction front) to form fresh lithiated silicon, a-$Li_\eta Si$. This process at the c-Si/a-$Li_\eta Si$ interface involves breaking of silicon−silicon bonds and formation of lithium−silicon bonds. Overall, this lithiation process causes lithiated silicon to grow at the expense of the crystalline silicon and metallic lithium.

We now propose a model to quantify the relationship between the measured potential and the applied current density, accounting for the motion of the phase boundary. To do so, we adopt a modified version of the Deal−Grove model for thermal oxidation of c-Si.[38] In the model, the concentration of lithium in the lithiated phase is a function of position, y (Figure 3). We take the reference state as that of amorphous lithiated silicon of a given composition, $Li_\eta Si$, in metastable "equilibrium" with crystalline silicon. In the current state, the composition becomes $Li_{\eta+\delta}Si$, where δ is a function of position y in the silicon electrode.

Lithiation is driven by the externally applied voltage or current density and involves three kinetic processes: the redox reaction at the electrolyte/a-$Li_\eta Si$ interface, the diffusion of lithium through the a-$Li_\eta Si$ phase, and the reaction at the a-$Li_\eta Si$/c-Si interface. The three kinetic processes are concomitant and are in series; any of these processes may be rate-limiting or they may occur at comparable rates such that multiple processes govern the lithiation process.

Associated with the redox reaction, $Li^+ + e^- = Li$, we take the flux through the electrolyte/a-$Li_\eta Si$ interface, J_1, as given by the Butler−Volmer equation

$$J_1 = \frac{i_0}{q}\left[\exp\left(-\frac{\alpha F}{RT}[\Phi - \Phi_{\mathrm{eq}}{}^{\mathrm{curr}}]\right) - \exp\left(\frac{[1-\alpha]F}{RT}[\Phi - \Phi_{\mathrm{eq}}{}^{\mathrm{curr}}]\right)\right] \quad (2)$$

where i_0 is the exchange current density, q is the elementary charge, α is the charge transfer coefficient, F is Faraday's constant, R is the ideal gas constant, T is the temperature, Φ is the potential of the electrode (i.e., the measured voltage), and $\Phi_{\mathrm{eq}}{}^{\mathrm{curr}}$ is the equilibrium potential in the current state, corresponding to the lithium concentration in the electrode near the electrolyte/a-$Li_\eta Si$ interface. Henceforth, we will use $\alpha = 1/2$ for simplicity.

In the lithiated phase, $\eta + \delta$ is the number of lithium atoms hosted by each silicon atom. We regard η as a constant and δ as a small deviation, $\delta \ll \eta$. As a result, the diffusion of lithium atoms in the lithiated silicon phase is driven by the position-dependence of the composition, $\delta(y)$. Let C be the concentration of lithium in the lithiated phase (i.e., the amount of lithium per unit volume of the lithiated phase). The concentration of lithium in this phase relates to the composition by $C = (\eta + \delta)/\Omega_{\mathrm{Li}\eta\mathrm{Si}}$, where $\Omega_{\mathrm{Li}\eta\mathrm{Si}}$ is the atomic volume of the lithiated phase. We take the flux, J_2, to be driven by the gradient in the concentration of lithium through the thickness of the lithiated silicon

$$J_2 = -D\frac{\partial C}{\partial y} \quad (3)$$

where D is the diffusivity of lithium in the lithiated silicon. Because $\delta \ll \eta$, D is taken to be a constant, independent of the concentration. In the steady state, the flux is independent of the position, and the concentration varies linearly in the position, so that $J_2 = D(C_1 - C_2)/y_0$, where C_1 is the concentration of lithium in the lithiated silicon at the interface between the electrolyte and the lithiated silicon, C_2 is the concentration of lithium in the lithiated silicon at the interface between the lithiated silicon and crystalline silicon phases, and y_0 is the thickness of the lithiated silicon.

At the interface between the lithiated silicon and the crystalline silicon phases, a chemical reaction occurs, as given by eq 1. The reaction is driven by the excess lithium δ_2 in the lithiated silicon at this interface. The rate of reaction controls the flux of lithium across the interface, and we take the corresponding lithium flux to be given by the first-order relation

$$J_3 = k\frac{\delta_2}{\Omega_{\mathrm{Li}_\eta\mathrm{Si}}} \quad (4)$$

where k is the rate of the reaction.

Using the Nernst equation, we can relate the equilibrium potential $\Phi_{\mathrm{eq}}{}^{\mathrm{curr}}$ to the excess lithium δ_1 in the lithiated silicon at the interface with the electrolyte

dx.doi.org/10.1021/nl302841y | Nano Lett. 2012, 12, 5039−5047

$$\Phi - \Phi_{eq}^{curr} = \Phi - \Phi_{eq}^{ref} + \frac{RT}{F}\left[\frac{\delta_1}{\eta(\eta+1)}\right] \quad (5)$$

where Φ_{eq}^{ref} is the equilibrium potential of a-Li$_\eta$Si in the reference state ($\delta = 0$).

With eqs 2−5, we can derive a relation between the applied current density, i, and the measured potential, Φ, in the steady state. For the full derivation of this relation, please see the Supporting Information. The result of this derivation is:

$$\frac{i}{i_0} = 2\sinh\left\{-\frac{F}{2RT}\left(\Phi - \Phi_{eq}^{ref} + \frac{RT}{F}\left[\frac{\Omega_{Li_\eta Si}}{q\eta(\eta+1)}\left(1 + \frac{ky_0}{D}\right)\frac{1}{k}i\right]\right)\right\} \quad (6)$$

It is important to note that there are three intrinsic time scales in this model: $qy_0\eta/i_0\Omega_{Li\eta Si}$, y_0^2/D, and y_0/k, associated with the electrolyte/electrode surface reaction, the diffusion through the a-Li$_\eta$Si layer, and the reaction at the a-Li$_\eta$Si/c-Si interface. There is also a time scale $qy_0\eta/i\Omega_{Li\eta Si}$ associated with the applied current density. These four time scales form three dimensionless groups: $i_0\Omega_{Li\eta Si}/kq\eta$, ky_0/D, and i/i_0. The parameter ky_0/D characterizes the relative rates of reaction at the a-Li$_\eta$Si/c-Si interface and diffusion through the a-Li$_\eta$Si phase. If $ky_0/D \gg 1$, the reaction at the a-Li$_\eta$Si/c-Si interface is fast, and eq 6 becomes

$$\frac{i}{i_0} = 2\sinh\left\{-\frac{F}{2RT}\left(\Phi - \Phi_{eq}^{ref} + \frac{RT}{F}\left[\frac{\Omega_{Li_\eta Si}}{q\eta(\eta+1)}\frac{y_0}{D}i\right]\right)\right\} \quad (7)$$

.

During a segment where the current density is prescribed as a constant, the thickness of the lithiated layer, y_0, increases with time. As a result, the potential, Φ, decreases with time. Such behavior is indeed observed in numerous electrochemical experiments, including the lithiation of amorphous sputtered silicon, and is indicative of a diffusion-limited process.

In contrast, if $ky_0/D \ll 1$, the diffusion of lithium through the lithiated phase is fast, and eq 6 becomes

$$\frac{i}{i_0} = 2\sinh\left\{-\frac{F}{2RT}\left(\Phi - \Phi_{eq}^{ref} + \frac{RT}{F}\left[\frac{\Omega_{Li_\eta Si}}{q\eta(\eta+1)}\frac{1}{k}i\right]\right)\right\} \quad (8)$$

Here, we take the reaction-rate, k, along a given crystal direction as a constant. In this limit, during a segment where the current density is prescribed as a constant, the potential, Φ, is likewise a constant. This observation is consistent with the previous discussion concerning our observed plateaus in potential, that is, this reaction-limited situation corresponds to a moving phase boundary.

Another possible limit of eq 6 occurs when the applied current density is very small such that $\{[\Omega_{li_\eta Si}/q\eta(\eta+1)](1 + ky_o/D)(1/k)i\} \ll 1$, giving

$$\frac{i}{i_0} = 2\sinh\left[-\frac{F}{2RT}(\Phi - \Phi_{eq}^{ref})\right] \quad (9)$$

that recovers the Butler−Volmer equation. It should be noted that the relative rates of diffusion and reaction at the a-Li$_\eta$Si/c-Si interface are irrelevant in this limit. Instead, both of these rates must be fast compared to the applied rate of insertion. Once again, during a segment where the current density is prescribed as a constant, the potential, Φ, is likewise a constant. This limit is known in literature as a process limited by the rate of the "surface reaction".[39]

Figure 4 demonstrates the effects of varying the intrinsic dimensionless parameters ky_0/D and $i_0\Omega_{Li\eta Si}/kq\eta$ for a fixed

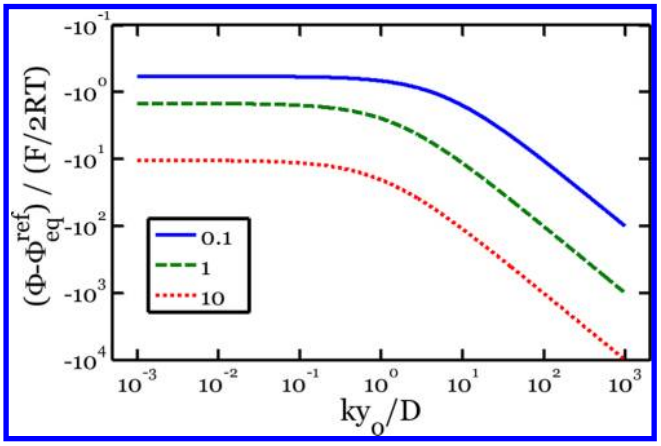

Figure 4. Potential predicted from kinetic model as a function of the dimensionless constant ky_0/D. The various curves represent different values of the dimensionless constant $i_0\Omega_{Li\eta Si}/kq\eta$. In this simulation, $i/i_0 = 1$.

value $i/i_0 = 1$. To produce this figure, we have solved eq 6 for the potential, Φ, for given values of the dimensionless constants. The various curves represent different values of the dimensionless constant $i_0\Omega_{Li\eta Si}/kq\eta$. During an electrochemical experiment at a constant current density, the thickness of the lithiated layer, y_0, will increase in time. Thus, the horizontal axis is representative of time during such an experiment. The transition from a reaction-controlled to a diffusion-controlled process can clearly be seen as ky_0/D increases. Also, larger values of $i_0\Omega_{Li\eta Si}/kq\eta$ indicate a slower rate of reaction at the interface between the lithiated silicon and the crystalline silicon, which results in larger values of overpotential, $|\Phi - \Phi_{eq}^{ref}|$.

We should also remark that within this model it is impossible to separate the contributions of the reactions at each interface from a single experiment. This is evident if we take the further limit of eq 8 for which $i \ll i_0$

$$\Phi - \Phi_{eq}^{ref} = -\frac{RT}{F}\left[\frac{\Omega_{Li_\eta Si}}{q\eta(\eta+1)}\frac{1}{k} + \frac{1}{i_0}\right]i \quad (10)$$

.

From eq 10, it is clear that if one reaction is much faster than the other, the measured relation between i and Φ gives information on the slower process. If both contributions in brackets are comparable, a single measurement relating i and Φ does not give distinct information on both i_0 and k. It may be possible, however, to quantify the individual contributions of the reactions at these interfaces from a set of multiple experiments in which one of these parameters is constant (or does not exist). For instance, one could measure the velocity of the phase boundary in lithium−silicon diffusion couples for silicon wafers of various orientations. This experiment would

dx.doi.org/10.1021/nl302841y | Nano Lett. 2012, 12, 5039−5047

give information on the parameter k, as the parameter i_0 associated with the redox reaction is unimportant. In another experiment, amorphous silicon samples could be examined. In these amorphous silicon samples, the electrode is a single phase with a continuous variation in the lithium concentration during lithiation. Hence, only diffusion and the redox reaction at the electrolyte/electrode contribute to the kinetics of the insertion process. Thus, experiments could be performed to carefully characterize $i_0(C)$ near the compositions of interest. Furthermore, a set of multiple experiments in which i_0 is a constant but k varies would give information on both parameters. We believe this latter situation applies to our experiments, as k depends on the crystallographic orientation, while i_0 is the same during each experiment.

We now apply the kinetic model to our experimental data. Upon close examination of all of our data, we have found that the majority of the nonzero constant current segments produce extremely flat profiles in potential with time (see for instance, Figure 1). The only exception to flat potential profiles occurred in some of the {100} and {111} samples during the largest current density used, 100 μA/cm^2. In these anomalous segments, the potential increased with time (Supporting Information Figures S1, S2). As mentioned in the previous section, if the lithiation process were controlled by diffusion through the lithiated silicon phase, the potential would decrease with time. Thus, we do not believe that the lithiation process is controlled by diffusion during these segments. We are uncertain about the precise origin of these upward sloping potentials, although they may correspond to some lithium from a-Li$_\eta$Si being consumed by the formation of solid electrolyte interphase (SEI).

The data in Figure 2 and other experiments also suggest anisotropy in lithiation of crystalline silicon.[30−32] Recalling that the lithiated phase is amorphous, it is difficult to imagine a source of anisotropy if the kinetics of the lithiation process were dominated by the reduction reaction at the electrolyte/a-Li$_\eta$Si interface. One may argue that the redox reaction depends on the nature of the SEI that forms between the electrolyte and the specific electrode, potentially leading to anisotropy. However, it seems improbable that the structure and composition of this SEI are strongly affected by the crystal orientation of the silicon, as the lithiated silicon side of this interface becomes amorphous during the early stages of the lithiation process. In contrast, anisotropy seems natural if the reaction at the a-Li$_\eta$Si/c-Si interface contributes to the overall kinetics of the lithiation process. For this reaction to advance, cooperative rearrangement of atoms must occur, involving breaking and reforming bonds. Surfaces of silicon in various crystallographic orientations have drastically different atomic structures, which can readily result in different rates of reaction on these different surfaces. For instance, such anisotropy has been observed in the rate of thermal oxidation of silicon of various crystal orientations.[40,41] Thus, we believe that the reaction at the a-Li$_\eta$Si/c-Si interface must contribute to the observed relationship between current density and potential as shown in Figure 2.

As previously mentioned, it is impossible to separate the contributions of the reactions at each interface from a single experiment. However, we believe that i_0 is independent of crystal orientation, while k is a function of crystal orientation. Since we have experiments for various crystal orientations of the silicon, we can fit both i_0 and k. To do so, we have written in a program in Matlab to solve eq 8 for a given k and i_0 to produce a relationship between the applied current densities and predicted potentials. We have then performed a least-squares fit between the measured and predicted potentials to find the appropriate values of k for each orientation and i_0. The parameters used in this simulation are given in Table 1. The

Table 1. Parameters Used in Simulations and Calculated Results[a]

parameter	value
T	20 °C
η	3.5[36]
$\Omega_{Li3.5Si}$	6.91×10^{-29} m^3 [37]
Φ_{eq}^{ref}: ⟨110⟩	149.2 ± 2.33 mV
Φ_{eq}^{ref}: ⟨111⟩	129.4 ± 2.41 mV
Φ_{eq}^{ref}: ⟨100⟩	128.3 ± 3.05 mV
$\beta = \Omega_{Li\eta Si}/\Omega_{Si}$	3.21[37]
σ_Y	1 GPa[18]
E_{Si}	160 GPa[46]
$E_{Li\eta Si}$	12 GPa[47]
$\nu_{Si} = \nu_{Li_\eta Si}$	0.22[46]
i_0*	0.45 A/m^2
k: ⟨110⟩*	1.63×10^{-10} m/s
k: ⟨111⟩*	7.05×10^{-11} m/s
k: ⟨100⟩*	2.54×10^{-11} m/s

[a]Results calculated from a fit of the model to the experimental data are denoted by *.

value used for η is a representative value found in other experiments under similar conditions.[36] Although this number may not be entirely accurate for our experiments, changing the value of η will only scale the predicted value of k by some constant numerical factor and will not affect the relative values of k for the various orientations. Also, the equilibrium potentials used in the simulation are the instantaneous values measured during the open circuit voltage segments in our experiments. It is important to note that the equilibrium potential associated with the {110} Si is approximately 20 mV larger than the other two orientations.

The results of this fit are shown in Table 1. Using these values, the predicted relationships between potential and current density are shown as dashed lines in Figure 2. The predictions from the fit agree well with the data. Both the calculated reaction rate at the a-Li$_\eta$Si/c-Si interface and the measured equilibrium potential are largest for {110} Si. Each of these characteristics contributes to the phase boundary moving "fastest" in the ⟨110⟩ direction for a given potential.

In the model, we have assumed a metastable equilibrium state, Li$_{3.5}$Si, as motivated by the observations of Li et al.[36] For small deviations from this composition, we can treat the quantities γ, D, i_0, and k as constants, independent of the concentration of lithium in the lithiated silicon phase. As a particular example, with the assumption that the lithiated phase is Li$_{3.5}$Si, we would expect the measured equilibrium potentials during open-circuit segments to be independent of the crystal orientation of the silicon. It was found, however, that the equilibrium potential for {110} Si was about 20 mV larger than for the other two orientations. It is possible that this discrepancy is due to a slightly different composition existing in the amorphous phase during the experiments on {110} Si. For instance, if the rate of the reaction at the a-Li$_\eta$Si/c-Si interface for {110} Si is fast compared to the insertion rate (i.e., applied current density), then the concentration of lithium in

dx.doi.org/10.1021/nl302841y | Nano Lett. 2012, 12, 5039−5047

the lithiated phase may be slightly smaller than that of the {100} and {111} orientations. This effect would result in a larger measured equilibrium potential, Φ_{eq}^{ref}, for {110} Si compared to the other orientations, which is consistent with the experiments. Such dependence of the composition of the metastable phase on the orientation of the crystalline phase is not considered in our model; Φ_{eq}^{ref} is simply taken as an input parameter measured from our experiments. This interplay may be important for the lithiation process, however, as it further amplifies the anisotropy along different crystal directions. Thus, once functions such as $\gamma(C)$, $D(C)$, $i_0(C)$, and so forth are more carefully characterized, they can be incorporated into the kinetic model to make it more complete. Still, we believe that the important physics associated with the initial lithiation of crystalline silicon have been captured in our kinetic model.

The model also provides some information of the value of the diffusivity of lithium in amorphous silicon. As discussed previously, it is evident from the flat potential profiles that diffusion through the lithiated phase is not the rate-limiting step. Using the values from the fit for i_0 and k, however, we can substitute various values of D into eq 6 and evaluate the effect on the potential profiles. The results are shown in Figure 5,

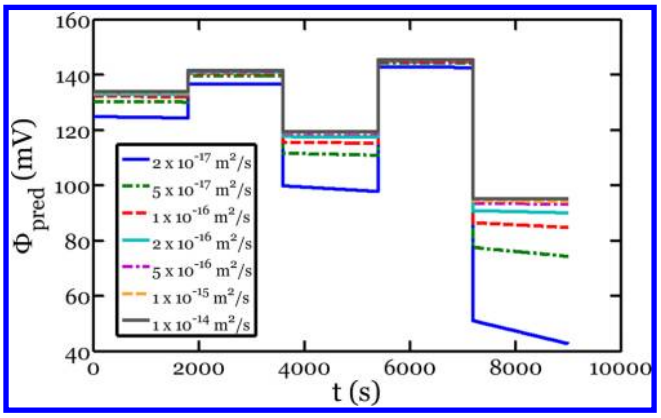

Figure 5. Predicted potential response versus Li/Li$^+$, Φ_{pred}, for a {110} Si wafer with initial lithiated thickness of 1 μm subject to the current loading shown in Figure 1. The various curves represent different hypothetical values of the diffusivity of lithium through the lithiated silicon phase.

where it is evident that the potential profiles would look drastically different if the diffusivity were as slow as 2×10^{-17} m^2/s. In comparison to the reaction-limited case, the measured potentials would be much smaller and would create profiles decreasing with time. Moreover, these slopes would increase in absolute value with current density, as given by eq 6. If we applied our kinetic model to a system that is rate-limited by diffusion through the electrode, we could fit eq 6 to the data to measure the value of diffusivity but as previously discussed, the overall kinetic process does not seem to be limited by diffusion through the amorphous layer during the initial lithiation of crystalline silicon. The results in Figure 5 can be used to estimate a lower bound on the diffusivity. Bearing in mind that the actual data are similar to the solid gray line in Figure 5, a reasonable estimate of the lower bound for the diffusivity of lithium in a-$Li_{3.5}Si$ is $D = 2 \times 10^{-16}$ m^2/s. In comparison to values in the literature, Ding et al. found a value of 1×10^{-16} m^2/s for nanocrystalline silicon particles using the galvanostatic intermittent titration technique (GITT), cyclic voltammetry (CV), and electrochemical impedance spectroscopy (EIS) at room temperature.[42] Similarly, Xie et al. found a value of 3×10^{-17}–3×10^{-16} m^2/s for sputtered amorphous silicon films using EIS at 20 °C.[43]

As a final comment, we have seen no evidence of diffusion-limited kinetics despite having lithiated samples to thicknesses on the order of micrometers. In contrast, typical nanostructured electrodes of silicon have feature sizes less than a few hundred nanometers.[7,9,14,15,44] Thus, under normal operating conditions, lithiation of crystalline silicon will be limited by the reaction of silicon and lithium at the reaction front, rather than by the diffusion of lithium through the amorphous phase.

We now use the measured velocities of the reaction fronts to quantify recent experimental observations. This analysis is performed under the framework of a previously developed model of concurrent reaction and plasticity; for more on this model, please see ref 33. The concurrent reaction and plasticity are simulated using the finite element program ABAQUS. Within the context of the program, the lithiation-induced volumetric expansion is simulated as thermal expansion, while deformation in the lithiated silicon is modeled by the elastic-plastic theory (J_2 plasticity).[45] The crystalline silicon is modeled as an elastic material. To simulate the movements of the reaction fronts, we prescribe a moving temperature field. To avoid computational singularity, the temperature front, which simulates the reaction front, is located within a thin shell, whose size is much smaller than the feature size of the nanopillar but is sufficiently larger than the mesh size. Such regularization is used to afford a compromise between computational cost and accuracy.

To illustrate this model in combination with our experimental data, we simulate the morphological evolution and stress development during the lithiation of crystalline silicon nanopillars of various axial orientations.[32] The black lines in the second column of Figure 6 show the crystal orientations of the sidewalls of these silicon nanopillars. The velocities of the fronts depend on the crystallographic orientation, with values given by our experiments at 120 mV (so-called "partial lithiation" by Lee et al.[32]). In particular, at this potential the relative velocities were found to be $V_{\langle 110\rangle} = 6.4V_{\langle 100\rangle} = 6.1V_{\langle 111\rangle}$. It is important to note that within this model, the absolute velocities of the reaction fronts are not important in developing the stress and deformation fields; only the relative velocities matter. In this simulation, we have used the following parameters: $\beta = \Omega_{Li_\eta Si}/\Omega_{Si} = 3.21$,[37] $\sigma_Y = 1$ GPa,[18] $E_{Si} = 160$ GPa,[46] $E_{Li_\eta Si} = 12$ GPa,[47] $\nu_{Si} = \nu_{Li_\eta Si} = 0.22$.[46] It should be noted that the modulus and Poisson's ratio of the crystalline Si phase are taken as independent of orientation. This approximation is made for simplicity of implementation into the ABAQUS model. The modulus used for the crystalline phase is that of polycrystalline silicon, which is a representative modulus of the core in an average sense. The pillars are modeled using plane–strain conditions, as motivated by experimental observations of a lack of growth in the axial direction.[32] Figure 6 shows the stress and morphology of the nanopillars after partial lithiation simulated using the procedure described above. The simulated anisotropic patterns agree extremely well with the experimental observations.[32]

Recently, it has been observed that under certain conditions these nanopillars will fracture anisotropically.[48] Moreover, Lee et al. surmised that this anisotropic fracture results from stress concentrations due to the anisotropic expansion of the nanopillars.[48] Here, we quantify this idea using ABAQUS and

dx.doi.org/10.1021/nl302841y | Nano Lett. 2012, 12, 5039–5047

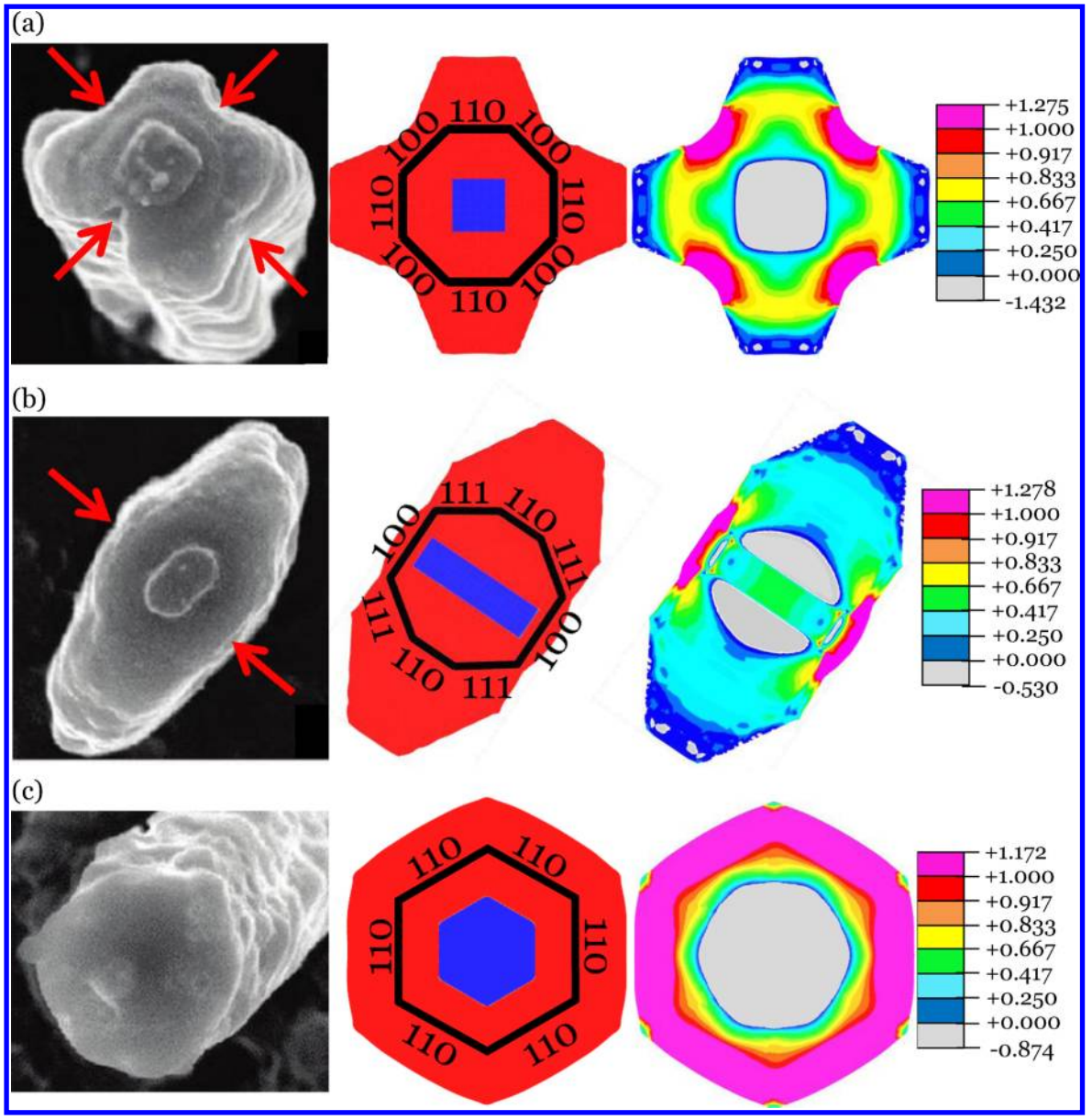

Figure 6. Comparison between experiments and finite element simulation of lithiation of crystalline silicon nanopillars of various axial orientations: (a) ⟨100⟩, (b) ⟨110⟩, and (c) ⟨111⟩. The first column shows the experimentally observed morphology after lithiation from Lee et al.[32] The red arrows indicate the fracture sites observed most frequently in experiments.[47] The second column shows simulated morphology at a certain stage of lithiation. The fully lithiated phase is given in red while the crystalline silicon phase is shown in blue. The black outline shows the initial shape in the simulation and the corresponding orientations of the crystal facets. The third column shows the maximum in plane stress at the same stage of lithiation. The pink regions have stresses exceeding the yield strength. The legend shows the stress in units of GPa.

our experimentally measured reaction front velocities. In Figure 6, we observe that for the ⟨100⟩ and ⟨111⟩ nanopillars the maximum principal tensile stress occurs at the locations midway between neighboring {110} planes. These locations are consistent with the fracture locations most frequently observed in the work of Lee et al.[48] Furthermore, we observe that the maximum tensile stress can exceed the yield strength due to the triaxiality of the state of stress at these locations. In the simulation of the ⟨111⟩ nanopillar, the state of stress was found to be approximately axisymmetric, implying that there should be little anisotropy in the locations of fracture. In the work of Lee et al., fracture was indeed observed at arbitrary locations albeit with a slightly higher incidence at locations between the {110} planes.[48] Thus, our simulations agree quite well with their experiments.

In conclusion, silicon can host a large amount of lithium, making it one of the most promising materials for anodes. Crystalline silicon is of particular importance due to its use in recent anode architectures such as nanowires, nanoporous structures, thin films, nanoparticles, and so forth. In this study, we have performed electrochemical experiments on {100}, {110}, and {111} crystalline silicon wafers. These experiments indicate the existence of a moving phase boundary for all three orientations, indicating that short-range processes at the a-$Li_\eta Si$/c-Si interface significantly contribute to the kinetics of the lithiation process. The velocity of this phase boundary was found to be faster for {110} silicon than for the other orientations. Using the measured velocities, we have implemented a model of concurrent reaction and plasticity into ABAQUS. This simulation accurately accounts for

dx.doi.org/10.1021/nl302841y | *Nano Lett.* 2012, 12, 5039−5047

anisotropic morphologies and fracture patterns developed in crystalline silicon nanopillars of various axial orientations. Furthermore, we have presented a kinetic model accounting for the redox reaction at the electrolyte/a-$Li_\eta Si$ interface, diffusion through the a-$Li_\eta Si$, and the chemical reaction at the a-$Li_\eta Si$/crystalline silicon interface. From this model, we have quantified the rates of reactions at the interfaces and have provided a lower bound for the diffusivity through the lithiated silicon phase. We believe that this model accounts for the pertinent physics in electrodes that undergo two-phase coexistence and will have further value beyond the silicon system. Thus, we hope this model will provide guidance for the design of future experiments and atomistic simulations.

Experimental Methods. Silicon wafers of three orientations, {100}, {110}, and {111}, were used as the working electrodes. The wafers were all doped with phosphorus and had similar and low resistivity (5−10 Ω·cm). Because of the low resistivity, the maximum ohmic drop in potential through the thickness of the wafer was calculated to be less than 50 μV for the current densities used in these experiments. The {100} and {110} wafers were 500 μm thick, and the {111} wafer was 250 μm thick. The wafers were cut into 6 cm × 1 cm sections.

The samples were cleaned with acetone and isopropanol. Next, they were placed into a sputter deposition system (AJA Int. ATC 1800). All sputtering targets used had a 50.8 mm diameter, and depositions were performed at room temperature (22 °C). First, the samples were plasma-cleaned in Ar at 20 mTorr and 24 W (RF) for 5 min. Then, a 50 nm thick layer of Ti was deposited, 3 mTorr of Ar at 100 W (DC) for 5 min, followed by a 250 nm layer of Cu, 5 mTorr of Ar at 200 W (DC) for 12.5 min. These layers serve as the current collector. On top of these layers, 500 nm of Si_3N_4 was deposited using plasma-enhanced chemical vapor deposition (Nexx Cirrus 150 PECVD) to prevent electrochemical reaction of Li with the Cu and Ti layers. During PECVD, a small region of the Cu layer was masked to allow for electrical contact with the electrode. It was observed in control experiments that no significant electrochemical signal was produced for an electrode coated with 500 nm of Si_3N_4; thus, the nitride served its purpose as a passivating layer.

Electrochemical cells were assembled in a glovebox (Vacuum Atmospheres HE-43) in an ultrahigh purity Ar atmosphere with less than 0.1 ppm moisture content. The Si wafer was incorporated as the working electrode into a homemade three-electrode electrochemical cell with lithium foil used as the counter and reference electrodes. One molar $LiPF_6$ in 1:1 (vol %) ethylene carbonate (EC)/diethyl carbonate (DEC) was used as the electrolyte (Novolyte Technologies). The cells were hermetically sealed inside the glovebox using paraffin wax and tested using a VersaSTAT 3 potentiostat (Princeton Applied Research) outside of the glovebox. The wafers were initially lithiated at a constant current density of 12.5 $\mu A/cm^2$ for 5 h followed by four other current densities: 6.25, 25, 50, and 100 $\mu A/cm^2$ applied in random order for 1 h each with a 30 min open-circuit segment between each imposed current density. To observe time-dependent effects in the experiments, all five current densities were then applied again (also in random order) for 30 min each. Finally, an open-circuit segment was applied for 30 min. For each sample, the two values of the measured potential corresponding to each current density were observed to be quite similar (usually within 1 mV), demonstrating that the results are quite reproducible. In other words, it does not seem that a time-dependent process such as continuous growth of the solid electrolyte interphase affects the measured potentials in a time-dependent manner. It is possible that the effect of the SEI is minimized because most of the growth may occur during the initial 5 h current segment. Still, it is important to note that the SEI will form during this experiment. This growth process may be different from cell to cell and may be one source of variation in the measured potentials from sample to sample. Additionally, it has been shown that below a potential of about 50 mV versus Li/Li+, amorphous $Li_\eta Si$ transforms to crystalline $Li_{3.75}Si$.[36] Thus, in an attempt to avoid this amorphous to crystalline phase transformation, the applied currents were selected such that the potential is maintained above 50 mV versus Li/Li^+.

To image the phase boundary, the samples were removed from the cell in the glovebox, rinsed in DEC, dried, and broken into fragments. These fragments were sealed in a container in the glovebox and immediately transferred to the SEM chamber. It was estimated that they were exposed to air for less than two minutes during the transfer process.

■ ASSOCIATED CONTENT

Ⓢ Supporting Information

Additional figures. This material is available free of charge via the Internet at http://pubs.acs.org.

■ AUTHOR INFORMATION

Corresponding Author

*E-mail: vlassak@seas.harvard.edu.

Notes

The authors declare no competing financial interest.

■ ACKNOWLEDGMENTS

This work is supported by the National Science Foundation through a grant on Lithium-ion Batteries (CMMI-1031161). This work was performed in part at the Center for Nanoscale Systems (CNS), a member of the National Nanotechnology Infrastructure Network (NNIN), which is supported by the National Science Foundation under NSF Award No. ECS-0335765. C.N.S. is part of Harvard University. M.P. acknowledges government support under and awarded by DoD, Air Force Office of Scientific Research, National Defense Science and Engineering Graduate (NDSEG) Fellowship, 32 CFR 168a.

■ REFERENCES

(1) Armand, M.; Tarascon, J. M. *Nature* **2008**, *451* (7179), 652−657.
(2) Service, R. F. *Science* **2011**, *332* (6037), 1494−1496.
(3) Ellis, B. L.; Lee, K. T.; Nazar, L. F. *Chem. Mater.* **2010**, *22* (3), 691−714.
(4) Marom, R.; Amalraj, S. F.; Leifer, N.; Jacob, D.; Aurbach, D. *J. Mater. Chem.* **2011**, *21* (27), 9938−9954.
(5) Zhang, W. J. *J. Power Sources* **2011**, *196* (1), 13−24.
(6) Beaulieu, L. Y.; Eberman, K. W.; Turner, R. L.; Krause, L. J.; Dahn, J. R. *Electrochem. Solid-State Lett.* **2001**, *4* (9), A137−A140.
(7) Chan, C. K.; Peng, H. L.; Liu, G.; McIlwrath, K.; Zhang, X. F.; Huggins, R. A.; Cui, Y. *Nat. Nanotechnol.* **2008**, *3* (1), 31−35.
(8) Peng, K. Q.; Jie, J. S.; Zhang, W. J.; Lee, S. T. *Appl. Phys. Lett.* **2008**, *93* (3), 033105.
(9) Takamura, T.; Ohara, S.; Uehara, M.; Suzuki, J.; Sekine, K. *J. Power Sources* **2004**, *129* (1), 96−100.
(10) Haftbaradaran, H.; Xiao, X. C.; Verbrugge, M. W.; Gao, H. J. *J. Power Sources* **2012**, *206*, 357−366.

(11) Yu, C. J.; Li, X.; Ma, T.; Rong, J. P.; Zhang, R. J.; Shaffer, J.; An, Y. H.; Liu, Q.; Wei, B. Q.; Jiang, H. Q. *Adv. Energy Mater.* **2012**, *2* (1), 68−73.
(12) Soni, S. K.; Sheldon, B. W.; Xiao, X. C.; Tokranov, A. *Scr. Mater.* **2011**, *64* (4), 307−310.
(13) Soni, S. K.; Sheldon, B. W.; Xiao, X. C.; Verbrugge, M. W.; Ahn, D.; Haftbaradaran, H.; Gao, H. J. *J. Electrochem. Soc.* **2012**, *159* (1), A38−A43.
(14) Baggetto, L.; Danilov, D.; Notten, P. H. L. *Adv. Mater.* **2011**, *23* (13), 1563−1566.
(15) Yao, Y.; McDowell, M. T.; Ryu, I.; Wu, H.; Liu, N. A.; Hu, L. B.; Nix, W. D.; Cui, Y. *Nano Lett.* **2011**, *11* (7), 2949−2954.
(16) Wu, H.; Chan, G.; Choi, J. W.; Ryu, I.; Yao, Y.; McDowell, M. T.; Lee, S. W.; Jackson, A.; Yang, Y.; Hu, L. B.; Cui, Y. *Nat. Nanotechnol.* **2012**, *7* (5), 309−314.
(17) Hertzberg, B.; Alexeev, A.; Yushin, G. *J. Am. Chem. Soc.* **2010**, *132* (25), 8548−+.
(18) Sethuraman, V. A.; Chon, M. J.; Shimshak, M.; Srinivasan, V.; Guduru, P. R. *J. Power Sources* **2010**, *195* (15), 5062−5066.
(19) Huang, J. Y.; Zhong, L.; Wang, C. M.; Sullivan, J. P.; Xu, W.; Zhang, L. Q.; Mao, S. X.; Hudak, N. S.; Liu, X. H.; Subramanian, A.; Fan, H. Y.; Qi, L. A.; Kushima, A.; Li, J. *Science* **2010**, *330* (6010), 1515−1520.
(20) Zhao, K. J.; Pharr, M.; Cai, S. Q.; Vlassak, J. J.; Suo, Z. G. *J. Am. Ceram. Soc.* **2011**, *94*, S226−S235.
(21) Zhao, K. J.; Pharr, M.; Vlassak, J. J.; Suo, Z. G. *J. Appl. Phys.* **2011**, *109* (1), 016110.
(22) Bower, A. F.; Guduru, P. R.; Sethuraman, V. A. *J. Mech. Phys. Solids* **2011**, *59* (4), 804−828.
(23) Wan, W. H.; Zhang, Q. F.; Cui, Y.; Wang, E. G. *J. Phys.: Condens. Matter* **2010**, *22* (41), 415501.
(24) Zhao, K. J.; Wang, W. L.; Gregoire, J.; Pharr, M.; Suo, Z. G.; Vlassak, J. J.; Kaxiras, E. *Nano Lett.* **2011**, *11* (7), 2962−2967.
(25) Obrovac, M. N.; Christensen, L. *Electrochem. Solid-State Lett.* **2004**, *7* (5), A93−A96.
(26) Li, H.; Huang, X. J.; Chen, L. Q.; Zhou, G. W.; Zhang, Z.; Yu, D. P.; Mo, Y. J.; Pei, N. *Solid State Ionics* **2000**, *135* (1−4), 181−191.
(27) Key, B.; Bhattacharyya, R.; Morcrette, M.; Seznec, V.; Tarascon, J. M.; Grey, C. P. *J. Am. Chem. Soc.* **2009**, *131* (26), 9239−9249.
(28) Key, B.; Morcrette, M.; Tarascon, J. M.; Grey, C. P. *J. Am. Chem. Soc.* **2011**, *133* (3), 503−512.
(29) Chon, M. J.; Sethuraman, V. A.; McCormick, A.; Srinivasan, V.; Guduru, P. R. *Phys. Rev. Lett.* **2011**, *107* (4), 045503.
(30) Liu, X. H.; Zheng, H.; Zhong, L.; Huan, S.; Karki, K.; Zhang, L. Q.; Liu, Y.; Kushima, A.; Liang, W. T.; Wang, J. W.; Cho, J. H.; Epstein, E.; Dayeh, S. A.; Picraux, S. T.; Zhu, T.; Li, J.; Sullivan, J. P.; Cumings, J.; Wang, C. S.; Mao, S. X.; Ye, Z. Z.; Zhang, S. L.; Huang, J. Y. *Nano Lett.* **2011**, *11* (8), 3312−3318.
(31) Goldman, J. L.; Long, B. R.; Gewirth, A. A.; Nuzzo, R. G. *Adv. Funct. Mater.* **2011**, *21* (13), 2412−2422.
(32) Lee, S. W.; McDowell, M. T.; Choi, J. W.; Cui, Y. *Nano Lett.* **2011**, *11* (7), 3034−3039.
(33) Zhao, K. J.; Pharr, M.; Wan, Q.; Wang, W. L.; Kaxiras, E.; Vlassak, J. J.; Suo, Z. G. *J. Electrochem. Soc.* **2012**, *159* (3), A238−A243.
(34) Yang, H.; Huang, S.; Huang, X.; Fan, F. F.; Liang, W. T.; Liu, X. H.; Chen, L. Q.; Huang, J. Y.; Li, J.; Zhu, T.; Zhang, S. L. *Nano Lett.* **2012**, *12* (4), 1953−1958.
(35) Boukamp, B. A.; Lesh, G. C.; Huggins, R. A. *J. Electrochem. Soc.* **1981**, *128* (4), 725−729.
(36) Li, J.; Dahn, J. R. *J. Electrochem. Soc.* **2007**, *154* (3), A156−A161.
(37) Zhao, K. J.; Tritsaris, A. G.; Pharr, M.; Wang, W. L.; Okeke, O.; Suo, Z. G.; Vlassak, J. J.; Kaxiras, E. *Nano Lett.* **2012**, *12* (8), 4397−4403.
(38) Deal, B. E.; Grove, A. S. *J. Appl. Phys.* **1965**, *36* (12), 3770−&.
(39) Li, J. C.; Xiao, X. C.; Yang, F. Q.; Verbrugge, M. W.; Cheng, Y. T. *J. Phys. Chem. C* **2012**, *116* (1), 1472−1478.
(40) Gonzalez, C.; McVittie, J. P. *IEEE Electron Device Lett.* **1985**, *6* (5), 215−218.
(41) Kao, D. B.; McVittie, J. P.; Nix, W. D.; Saraswat, K. C. *IEEE Trans. Electron Devices* **1987**, *34* (5), 1008−1017.
(42) Ding, N.; Xu, J.; Yao, Y. X.; Wegner, G.; Fang, X.; Chen, C. H.; Lieberwirth, I. *Solid State Ionics* **2009**, *180* (2−3), 222−225.
(43) Xie, J.; Imanishi, N.; Zhang, T.; Hirano, A.; Takeda, Y.; Yamamoto, O. *Mater. Chem. Phys.* **2010**, *120* (2−3), 421−425.
(44) Yamada, M.; Ueda, A.; Matsumoto, K.; Ohzuku, T. *J. Electrochem. Soc.* **2011**, *158* (4), A417−A421.
(45) Hill, R. *The Mathematical Theory of Plasticity*; Oxford University Press: Oxford, 1950.
(46) Freund, L. B.; Suresh, S. *Thin Film Materials: Stress, Defect Formation and Surface Evolution*; Cambridge University Press: Cambridge, U.K., 2003.
(47) Hertzberg, B.; Benson, J.; Yushin, G. *Electrochem. Commun.* **2011**, *13* (8), 818−821.
(48) Lee, S. W.; McDowell, M. T.; Berla, L. A.; Nix, W. D.; Cui, Y. *Proc. Natl. Acad. Sci. U.S.A.* **2012**, *109* (11), 4080−4085.